CHEMICAL ENGINEERING TRANSACTIONS
VOL. 70, 2018
A publication of AIDIC
The Italian Association of Chemical Engineering
Online at www.aidic.it/cet
Guest Editors: Timothy G. Walmsley, Petar S. Varbanov, Rongxin Su, Jiří J. Klemeš

**ISBN** 978-88-95608-67-9; **ISSN** 2283-9216
DOI: 10.3303/CET1870116

# CFD Based Optimization of a $NO_X$ Removal Reactor

Attila Egedy[a,*], Norbert Miskoczi[a], Peng Yuan[b], Boxiong Shen[b]

[a]Institute of Chemical and Process Engineering, University of Pannonia, Veszprém H-8201, Hungary
[b]School of Energy and Environmental Engineering, Hebei University of Technology, Tianjin 300401, P. R. China
egedya@fmt.uni-pannon.hu

$NO_x$ gases are by-products of numerous technologies, such as nitric-acid production, but are also present in the flue gas. $NO_x$ is known to have a strong negative environmental impact; therefore, its reduction in process technologies is a top priority. Various technologies have been developed for the reduction of the $NO_x$ content, including absorption, adsorption and catalytic removal. The kinetics and hydrodynamics pay a key role in the efficiency of all processes above. For instance, the geometry and the position of the inlet gas distributor have a significant effect on the Fenton reagent absorption process. In this case, the optimal solution must provide homogeneous feed gas distribution in the vessel, which leads to maximal phase contact, therefore improved removal efficiency. The objective of this work is the CFD based optimization of a laboratory scale $NO_x$ removal absorption vessel. Different inlet geometries were designed and evaluated using CFD modeling. 12 geometries with 4 nozzle number (1, 4, 37 and 64), and 3 inlet areas (5.8e-5 $m^2$ (50 %), 1.2e-4 $m^2$ (100 %) and 1.7e-4 $m^2$ (150 %)) were simulated, in COMSOL CFD environment. The geometries were evaluated based on the analysis of the outlet variables (gas volume fractions, well-mixed areas). The 64-nozzle construction with medium inlet area gave the best performance, which has the maximal averaged well-mixed area from all constructions.

## 1. Introduction

The environmental problems related to industrial production activities became a major concern in the last few decades. The CO, $CO_2$, and $NO_x$ emissions are regulated in governmental level to promote the development of environmentally friendly technologies. The result of such an effort is the separation and utilization of $NO_x$ content of flue gases as starting material in another operation in the production line or as an end-product. This method has more application areas in the case of carbon oxides. Besides the industrial, the residential emission is also significant. There are different processes for $NO_x$ removal from gas streams. Ultimately, these technologies can be divided into two groups: physical or chemical sorption, and reactions.

In the case of absorption, the flue gas is contacted with liquid phase reagent. In addition to physical absorption, in the liquid phase, chemical reactions also took place. Zhao et al. (2014) investigated experimentally the removal of nitrogen and sulfur oxides in bubbling reactor using Fenton reagent, and the operational parameters (initial pH concentration, and flow rates) were optimized. 100 % removal efficiency was achieved for $SO_2$, and 90 % for $NO_x$ removal at 55 °C, and pH 3. However, the flue gas composition might vary, as a function of combustion conditions and fuel type, hence, other pollutants (for example Hg) can be present. Therefore, the absorber system must be designed and optimized as a function of flue gas composition. Zhao et al. (2017) used NaClO as an additive in their Fenton based complex oxidant to successfully extract $Hg^0$, $NO_x$, and $SO_2$ from the flue gas. The achievable results strongly depend on the reagent concentration and ratio. They applied a fixed bed reactor and reported removal efficiencies of 100 % for $SO_2$, 81 % for NO and 91 % for $Hg^0$ under optimal conditions. Deshwal and Kundu (2015) applied Fe(II) ions with EDTA and activated carbon for the simultaneous removal of $SO_2$ and NO. With the composite system, 100 % $SO_2$ removal and approximately 100 % $NO_x$ removal was achieved. According to the observations, the activated carbon probably provides synergic adsorption effect, so it improves the absorption processes.

Beyond the reagent nature, other factors might also influence the $NO_x$ removal process. Numerous studies show that the use of UV light affects the process through photocatalytic mechanisms. Su et al. (2016) carried out a response surface method optimization of a UV/$H_2O_2$ system. With the optimized operation parameters (including

Please cite this article as: Egedy A., Miskolczi N., Yuan P., Shen B., 2018, Cfd based optimization of a nox removal reactor , Chemical Engineering Transactions, 70, 691-696 DOI:10.3303/CET1870116

Fe, $H_2O_2$, NO, temperature, $O_2$ concentration, flue gas flow) 90 % $NO_x$ removal efficiency was found, which is acceptable in low-temperature removal technologies. Mills and Elouali (2015) examined of photocatalytic reactions of $TiO_2$ based materials. They showed that the UV exposure time is the most important process parameter, and also, achieved a total NO to $NO_2$ conversion during a 5-hour long ISO standard test. Yu et al. (2011) used $C_3H_8$ reagent in a monolith reactor, equipped with $TiO_2$, Pd, and Pt catalyst system and achieved 90 % optimal removal efficiency, however, at higher temperatures the removal efficiency dropped to 73 % due to less efficient $NO_x$ and $C_3H_8$ adsorption. Ângelo et al. (2013) published a review paper about photocatalytic processes, where the potential of $TiO_2$ based system, as well as the impact and optimization of operating parameters, were compared and summarized. The conclusion was that the inlet conditions, the catalyst preparation, and the reaction conditions are the key design parameters for high-performance $NO_x$ removal systems.

Another pathway for $NO_x$ removal from the flue gas streams is the catalytic degradation, referred as Selective Catalytic Reduction – SCR. Fu et al. (2015) applied an Mn and Cu based catalyst for $NO_x$ removal and achieved high removal efficiencies, which justifies the considerable potential of SCR. As a drawback, the reactions require elevated temperatures (over 150 °C).

Lasek et al. (2013) pointed out that probably the combination of the advantages of traditional (thermal, absorption and catalytic removal) and photocatalytic processes will be the right path to follow for the design of increased $NO_x$ removal efficiencies. Chen et al. (2017) proposed a combined catalytic/absorption method and reached 95.6 % peak removal efficiency, which beyond the limits of traditional technologies, although the operating temperature was between 160-240 °C. There is some novel, promising technologies that deliver increased removal efficiency under milder conditions. Wang et al. (2017) achieved high removal efficiency for $NO_x$ as well as for other pollutants using electrolytic processes. They presented the influencing factors and discussed the scale-up concepts of the proposed method.

While most studies focus on the experimental investigation, there is high potential in the mathematical model-based techniques. Model-based approaches can be applied from the technology design through operation to control. Such a study was presented by Chen and Tan (2012), who examined an $NH_3$ based SCR system. A 3D model of the catalytic filter was developed and validated, which was used then for the optimization of the operating parameters (temperature, reagent usage, residence time). By exploiting the predictive power of the process model, the optimal removal of NO reached 99.93 %. Relevant information, for example, the gas turbine $NO_x$ and CO emission could be predicted using a detailed model and used at industrial scale, where the simulation time availability is limited. Kanniche (2009) showed a predictive model for emission levels. The CFD calculations were performed with simplified kinetics and were post-treated using a reactor network simulator, which involved a detailed kinetic description. The effects process conditions were evaluated, and the model was validated using a laboratory scale device.

As it was evidentiated by numerous studies, the most important factors in $NO_x$ removal technologies are the reagent, catalyst, and the operation parameters. However, the system geometry is the key aspect of the design stage. Yang et al. (2016) applied CFD simulations to characterize the operation of a multiphase airlift membrane bioreactor for $NO_x$ removal. The kinetics, oxygen transport mechanism, and rheology were also considered. The membrane construction was optimized based on the CFD model, which lead to increased $NO_x$ removal efficiency was achieved (>90 %).

In this study, a $Fe^{2+}/H_2O_2$ Fenton system is evaluated. The reactor system is operated at room temperature in a gas-fluid absorption system. The primary goal of this study is the development of multiphase CFD models and the model-based optimization of the inlet nozzle configuration to maximize the gas-liquid mixing in the vessel. Presumably, this leads to optimal device operation by providing maximal gas-liquid contact area possible.

## 2. Model description

Figure 1a shows three representatives of nozzle construction examples, whereas Figure 1b represents the full reactor geometry. The device is 0.415 m long and has a diameter of 0.0865 m. Geometries with three different inlet areas and nozzle numbers are simulated. Table 1 lists the applied parameters for each simulation (case). 1e-5 $m^3/s$ (600 ml/min) gas flow rate was used for all the simulations.

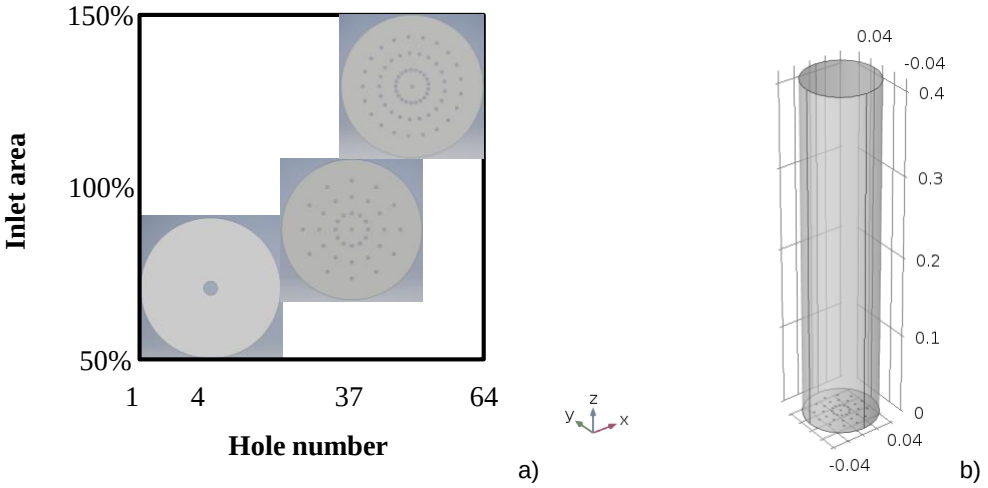


*Figure 1: a) Representation of the evaluated geometries b) Full geometrical model of the reactor*

*Table 1: The simulated geometries r – nozzle radius, $A_1$ – nozzle area (1 nozzle), $A_2$ – inlet area, n – the number of nozzles)*

| case | 1 | 2 | 3 | 4 | 5 | 6 | 7 | 8 | 9 | 10 | 11 | 12 |
|---|---|---|---|---|---|---|---|---|---|---|---|---|
| r | 6,1E-03 | 3,0E-03 | 1,0E-03 | 7,8E-04 | 4,3E-03 | 2,2E-03 | 7,1E-04 | 5,4E-04 | 7,4E-03 | 3,7E-03 | 1,2E-03 | 9,3E-04 |
| n | 1 | 4 | 37 | 61 | 1 | 4 | 37 | 64 | 1 | 4 | 37 | 64 |
| $A_1$ | 1,2E-04 | 2,9E-05 | 3,1E-06 | 1,9E-06 | 5,8E-05 | 1,5E-05 | 1,6E-06 | 9,1E-07 | 1,7E-04 | 4,4E-05 | 4,7E-06 | 2,7E-06 |
| $A_2$ | 1,2E-04 | 1,2E-04 | 1,2E-04 | 1,2E-04 | 5,8E-05 | 5,8E-05 | 5,8E-05 | 5,8E-05 | 1,7E-04 | 1,7E-04 | 1,7E-04 | 1,7E-04 |

k-ε turbulence model was used for the momentum balance calculation. The two-fluid model was used for the calculation of the gas and liquid phases with the following assumptions.

- The gas holdup is negligible, compared to the liquid holdu[.
- The viscous drag and pressure forces govern the bubble movement.
- The two phases share the same pressure field.

Then, the momentum and continuity equations for the two phases can be combined, and a gas phase transport equation is used to track the volume fraction of the bubbles. Eq(1) is the momentum equation.

$$\Phi_l \rho_l \frac{\partial u_l}{\partial t} + \Phi_l \rho_l u_l \cdot \nabla u_l = -\nabla p + \nabla \left[ \Phi_l (\mu_l + \mu_T) \left( \nabla u_l + \nabla u_l^{\,T} - \frac{2}{3} (\nabla \cdot u_l) I \right) \right] + \Phi_l \rho_l g + F \qquad (1)$$

Where:

- $u_l$ is the velocity vector [m/s]
- p is the pressure [Pa]
- Φ is the phase volume fraction [1] (l refers to a liquid, while g refers to gas)
- ρ is the density [kg/m$^3$]
- g is the gravity vector [m/s$^2$]
- F is any additional volume force [N/m$^3$]
- $\mu_l$ is the dynamic viscosity of the liquid [Pa•s]
- $\mu_T$ is the turbulent viscosity [Pa•s]

The continuity equation is Eq(2):

$$\frac{\partial}{\partial t} (\rho_l \Phi_l + \rho_g \Phi_g) + \nabla \cdot (\rho_l \Phi_l u_l + \rho_g \Phi_g u_g) = 0 \qquad (2)$$

Finally, the gas phase transport equation takes the form:

$$\frac{\partial \rho_g \Phi_g}{\partial t} + \nabla \cdot \rho_g \Phi_g u_g = -m_{gl} \qquad (3)$$

Where $m_{gl}$ is the gas-liquid mass transfer rate [kg/($m^3$·s)]. The gas velocity is the origin of the liquid, slip, and drift velocities (where it is acceptable). The first simulation was carried out on multiple meshes, and the numerical grid for the further simulations was chosen base on the outcome of this mesh independence study. At first, the gas volume fraction was calculated through the vessel. Finally, the different constructions were compared to each other based on the gas volume fraction distribution in the reactor.

## 3. Results and discussion

Figure 2 shows the gas volume fractions at 0.0075, 0.1075, 0.2075, 0.3075 and 0.4075 m-s (section 1 to 5 respectively) from the bottom of the reactor in case 1-to 4.

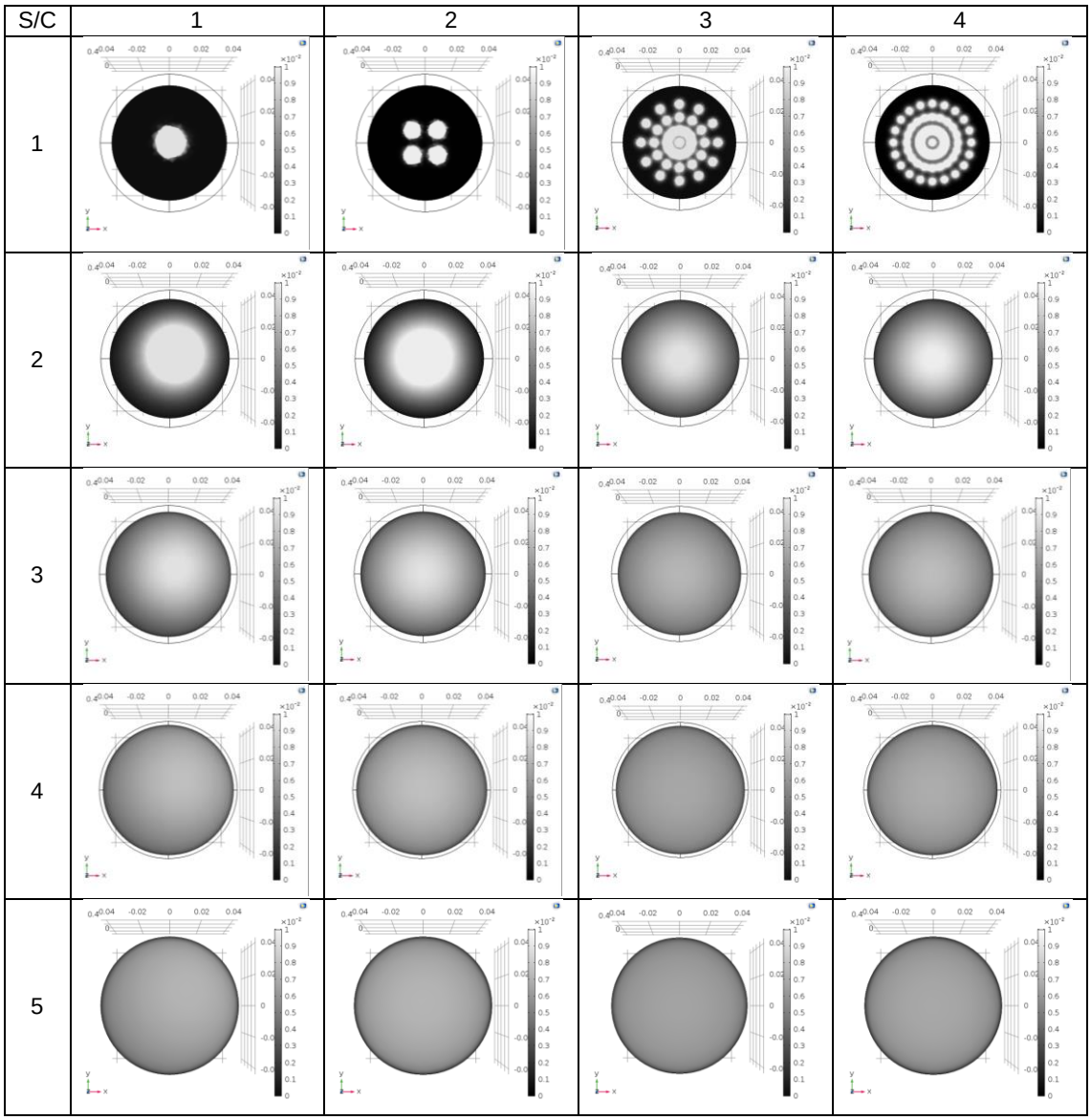


*Figure 2: Gas volume fractions in different cross sections of the reactor (from top to bottom 0.0075, 0.1075, 0.2075, 0.3075 and 0.4075 m) for the 1.16e-4 $m^2$ area cases (case 1 to 4), S refers to the section (in rows), whereas C refers to the case (in columns).*

In the first section, the effect of the different inlet nozzle geometries can be seen. The first, second and third sections (which are the most influenced by the nozzles constructions) exhibits the biggest difference. In case 1 and 2 the gas phase is concentrated, whereas in case of 3 and 4 is better distributed. This translates to higher performance of cases 3 and 4 in the reaction since the distribution of the gas took place in the first half of the reactor. Image processing was applied for the quantification of CFD simulation results. In the first step, the

images were loaded to the workspace. Then, the red color space of the picture (used for the visualization of CFD results, because it has the most significant changes in the pictures) was converted to greyscale, and a smaller region of interest (ROI) was applied on it. Using a threshold value (25), the number of the pictures was calculated, in which the gas flow was significant. Then, the well-mixed ratio (number of well-mixed pixels/number of all pixels in the reactor cross-section area) was averaged in each construction. Figure 3a shows the video processing results for case 1 section 1 and Figure 3b for case 1 section 5, whereas Figure 3c presents all the results.

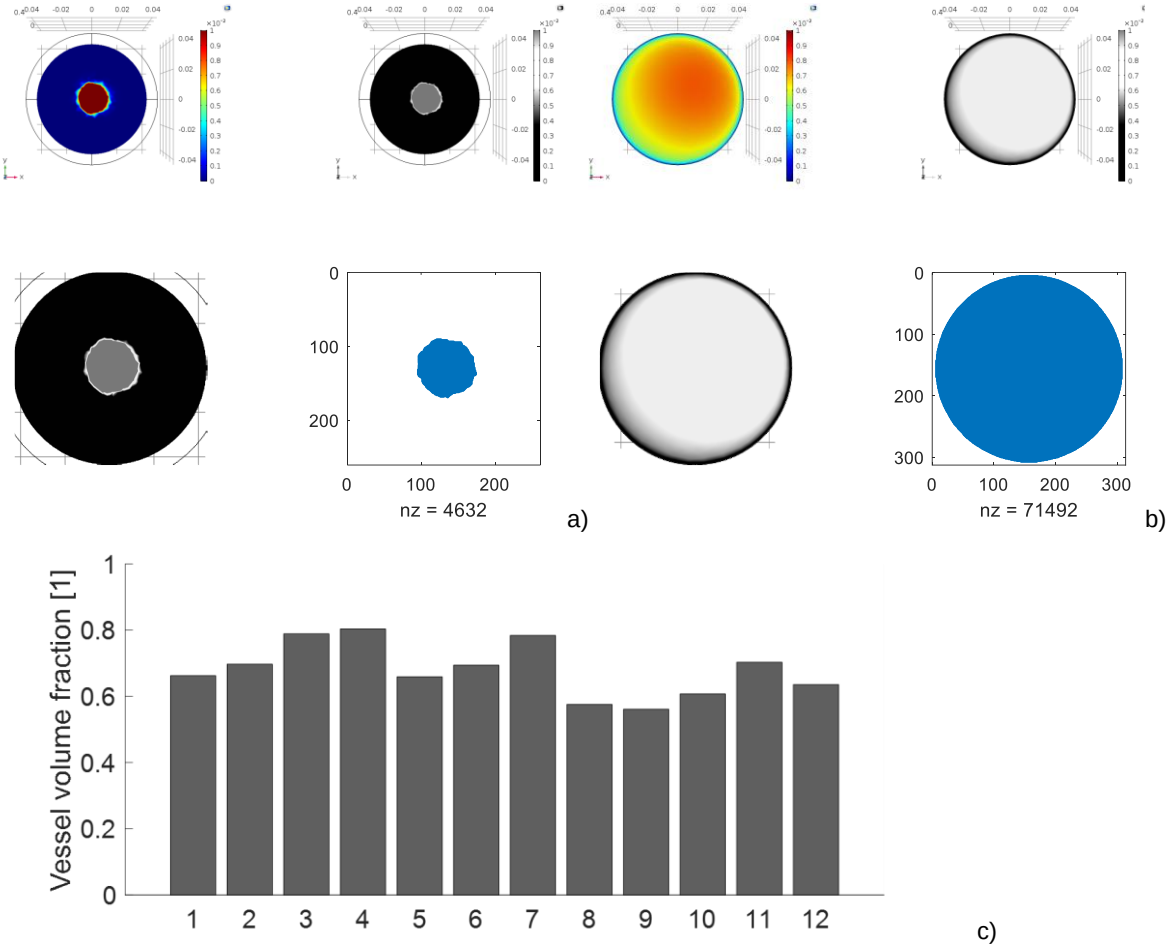


*Figure 3: a) The results of the image processing for case 1 section 1, b) The results of the image processing for case 1 section 5 c) he averaged volume fraction results for every case*

Figure 3a and b supports that the chosen threshold value is acceptable, and reflects correctly the well-mixed areas. From Figure 3c the following conclusions can be drawn. All constructions have vessel volume fraction above 0.5. The minimal vessel volume fraction was found in case 9 which has the largest inlet area with one inlet. The optimum value is found in case 4 which corresponds to medium inlet area with 64 nozzles. Vessel volume fractions above 0.7 (case 3,4,7, and 11) are considered acceptable. The positive impact of using 64 nozzles decreases with the increase of the overall inlet area. Improved results are achieved by more uniform inlet nozzle dispersion through the inlet area (cases with 37, or 64 nozzles).

## 4. Conclusions

A detailed multiphase turbulent CFD model of a gas-liquid laboratory scale $NO_x$ removal reactor was developed. Four different geometries and 3 inlet areas were developed and simulated considering constant gas flow rate. The 12 cases were evaluated based on sections of the gas volume fractions. The cross sections were assessed using image processing methods, and the vessel volume fractions were also calculated. Based on the results, the optimal construction was found, which has 64 nozzles, the largest nozzle number applied in this study. The

medium inlet area was sufficient for the phase contact in this case. The 37 nozzle geometry has similar efficiency however from the point of view of reactor manufacturing this simpler geometry could be a better choice. Cost evaluation was not carried out, which work, is under development. Further research is required for the experimental validation of the simulation results. Also, the simulator can be extended with the integration of kinetic models, like the Fenton reactions, which would make the system suitable for the simulation of $NO_x$ removal process. Application of approximate compartment model can be relevant in the industrial scale simulations because of their reduced computational burden.

**Acknowledgments**

The authors acknowledge the Horizon 2020, Marie Curie Research and Innovation Staff Exchange (RISE) (MSCA-RISE-2014 (Flexi-pyrocat, No.: 643322)). Attila Egedy's research was supported by EFOP-3.6.1-16-2016-00015 Smart Specialization Strategy (S3) -Comprehensive Institutional Development Program at the University of Pannonia to Promote Sensible Individual Education and Career Choices project.
The financial support of MOL Nyrt. and Peregrinatio I. Foundations is gratefully acknowledged.
Peng Yuan's research was supported by Joint Doctoral Training Foundation of HEBUT (HW2017003) and Doctoral Innovation Project of Hebei Province (CXZZBS2017027).

**References**

Ângelo J., Andrade L., Madeira L. M., Mendes A., 2013, An overview of photocatalysis phenomena applied to $NO_x$ abatement. Journal of Environmental Management, 129, 522–539.

Chen C.T., Tan W.L., 2012, Mathematical modeling, optimal design and control of an SCR reactor for $NO_x$ removal. Journal of the Taiwan Institute of Chemical Engineers, 43(3), 409–419.

Chen L., Li Y., Zhao Q., Wang Y., Liang Z., Lu Q., 2017, Removal of $NO_x$ Using Hydrogen Peroxide Vapor over Fe/TiO2 Catalysts and an Absorption Technique. Catalysts, 7(12), 386.

Deshwal B.R., Kundu N., 2015, Simultaneous removal of NO and $SO_2$ from simulated flue gas using Fe (II) EDTA coupled with catalytic regeneration. European Journal of Applied Engineering and Scientific Research, 4(2), 10–19.

Fu Z., Guo M., Liu C., Ji N., Song C., Liu Q., 2015, Design and Synthesis Functional Selective Catalytic Reduction Catalyst for $NO_x$ Removal. Procedia Engineering, 121, 952–956.

Kanniche M., 2009, Modelling natural gas combustion in gas turbine: Coupling 3D combustion simulations with Chemical Reactor Network for advanced $NO_x$ predictions, Chemical Engineering Transactions, 18, 135-140

Lasek J., Yu Y.H., Wu J.C. S., 2013, Removal of $NO_x$ by photocatalytic processes. Journal of Photochemistry and Photobiology C: Photochemistry Reviews, 14(1), 29–52.

Mills A., Elouali S., 2015, The nitric oxide ISO photocatalytic reactor system: Measurement of $NO_x$ removal activity and capacity. Journal of Photochemistry and Photobiology A: Chemistry, 305(x), 29–36.

Su W., Lu P., Ma J., Wang M., Chang G., Tong Z., Song C., 2016, Research on the technology and mechanism of flue gas oxidation denitrification based on $H_2O_2$/UV system. Chemical Engineering Transactions, 55, 109–114.

Wang H., Tong Z., Yun Y., 2017, Research progress in flue gas denitrification technology based on oxidation theory, Chemical Engineering Transactions, 59, 175–180.

Yang M., Wei Y., Zheng X., Wang F., Yuan X., Liu J., Fan Y., 2016, CFD simulation and optimization of membrane scouring and nitrogen removal for an airlift external circulation membrane bioreactor. Bioresource Technology, 219, 566–575.

Yu Y.H., Pan Y.T., Wu Y.T., Lasek J., Wu J.C.S., 2011, Photocatalytic NO reduction with $C_3H_8$ using a monolith photoreactor. Catalysis Today, 174(1), 141–147.

Zhao Y., Wen X., Guo T., Zhou J., 2014, Desulfurization and denitrogenation from flue gas using Fenton reagent. Fuel Processing Technology, 128, 54–60.

Zhao Y., Hao R., Xue F., Feng Y., 2017, Simultaneous removal of multi-pollutants from flue gas by a vaporized composite absorbent. Journal of Hazardous Materials, 321, 500–508.